Journal of Structural Geology, Vol. 7, No. 1, pp. 83 to 102, 1985
Printed in Great Britain.

0191-8141/85 $03.00 + 0.00

Recent developments in centrifuge modelling of tectonic processes: equipment, model construction techniques and rheology of model materials

JOHN M. DIXON

and

JOHN M. SUMMERS

Experimental Tectonics Laboratory, Department of Geological Sciences,
Queen's University, Kingston, Ontario, K7L 3N6

(*Received* 23 *November* 1983; *accepted in revised form* 12 *April* 1984)

Abstract—The Experimental Tectonics Laboratory at Queen's University is equipped with a large-capacity centrifuge that is capable of subjecting tectonic models measuring 127 × 76 mm in plan and up to 51 mm in depth to accelerations as high as 20,000 ***g***. This high capacity greatly extends the range of potential model materials and permits the use of relatively stiff and/or brittle substances.

A number of new techniques of model construction have been devised, that permit internal and surface strain patterns and kinematic evolution to be monitored in detail. One particularly useful technique, which will find application in non-centrifuged experiments as well, allows the preparation of highly uniform anisotropic multilayers composed of alternating layers of Plasticine and silicone putty, with individual layer thicknesses as low as 20 μm and with controllable ratio between thicknesses of the relatively competent and incompetent units. Examples of models constructed using these new techniques are illustrated.

One particular type of the commonly used model material, silicone putty, has been subjected to a series of rheological tests. The results indicate that at strain rates in the range 10^{-6}–10^{-3} s^{-1} (applicable to the centrifuge experiments) the silicone putty exhibits power-law rheology with $n = 7 \pm 2$. At higher strain rates the material appears to tend towards linear behaviour.

Available rheological data and dimensional analysis using standard scaling laws and appropriate model ratios suggest that the microlaminated Plasticine–silicone putty multilayer is a suitable analogue, in centrifuged experiments, for interbedded sequences of indurate limestone and incompetent shale. The excellent degree of dynamic similitude attained is demonstrated by the realistic form of fold and fault structures developed in models constructed of this material.

INTRODUCTION

IN THIS paper we will review progress, to date, in a series of experimental studies in which the evolution of a range of large-scale tectonic structures has been investigated using the technique of centrifuge modelling. The work has been carried out using a 20,000 ***g*** centrifuge, recently installed in the Experimental Tectonics Laboratory at Queen's University. Our aims in this contribution are to describe the centrifuge facility, to discuss techniques of model construction and analysis and to report results of rheological testing of materials used in the experiments.

One particular technique of model construction may find general application in the field of tectonic modelling. The technique allows the interlayering of very thin sheets (20–100 μm) of Plasticine and silicone putty at a scale that simulates a realistic density of bedding planes within models designed to study the evolution of large-scale deformation structures in bedded sedimentary sequences.

THE CENTRIFUGE FACILITY

The centrifuge (Figs. 1 and 2) is capable of subjecting two specimens, each measuring 3.0 × 5.0 inches (76 × 127 mm) in plan by 2.0 inches (51 mm) thick (see Fig. 3), to accelerations up to 20,000 ***g***. The specimens are mounted in cavities milled in diametrically opposed positions in a solid, disc-shaped aluminium alloy rotor measuring 34 inches (864 mm) diameter by 3.5 inches (89 mm) thick. The bases of the specimens are located at a rotational radius of 13.75 inches (349 mm).

The rotor is directly coupled to a 30 h.p. A.C. motor, with power supplied through a variable-frequency SCR (silicon-controlled rectifier) drive unit. During start-up of the machine the rotation rate follows a preprogrammed ramp of 720 r.p.m. per min. Maximum acceleration of 20,000 ***g***, corresponding to 7200 r.p.m., can thus be achieved in approximately 10 min. Deceleration also follows a preprogrammed ramp, but at a lower rate.

The centrifuge rotor is supported by two sets of precision bearings and is contained within a cylindrical chamber 50 inches (1270 mm) in diameter by 12.25 inches (311 mm) deep, constructed of 1 inch thick steel plate, that serves as a safety barrier. Within the chamber, and concentric about the axis of rotation, are an aluminium shroud (for aerodynamic smoothness), and a cooling system composed of three helical coils of 5/8″ (16 mm) o.d. copper pipe.

The test specimens are held in the rotor cavities by high-strength alloy steel cover plates that are bolted to the rotor. Only the top surface of the model (facing radially inward) is exposed to view. During a centrifuge run, the progress of the experiment can be monitored via closed circuit television; a TV camera aimed through a

plexiglass port in the rotor chamber provides an oblique view of the model's top surface. Illumination is provided by a stroboscope, synchronized with the rotation of the rotor. Either of the two models may be viewed at will by manually varying the delay time between a one pulse-per-revolution trigger and the stroboscope flash. With surface grids and with oblique lighting to enhance relief, the surface deformation of the model can be easily monitored and is used as a guide to the state of internal deformation as an experiment proceeds. The TV signal can be recorded on a video cassette recorder.

The centrifuge facility also includes a Commodore PET 2032 (32 kbytes RAM) microcomputer system with disc drive and printer. The computer is connected to the centrifuge control panel via a Hewlett-Packard Multi-programmer and Interface and is used for a number of real-time control and data acquisition functions, including run times and g-levels and model and bearing temperatures.

An electrical slip-ring assembly, mounted on the rotor axis, provides connections to sensors such as thermocouples and strain gauges in the models. Each model cavity has eight electrical leads.

The centrifuge was designed and constructed by Genisco Technology Corp., Compton, California. It is their standard model 1075, with custom modifications in the form of rotor cavities, viewing port and cooling coils.

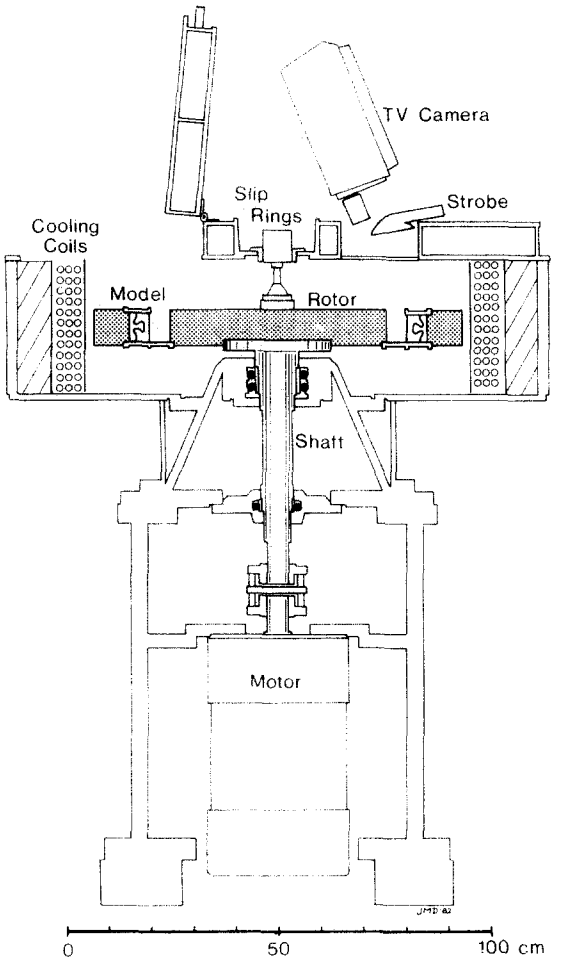

Fig. 2. Schematic cross-section of the centrifuge, showing diametrically opposed model chambers, TV viewing system, cooling coils, etc. (see text for complete description).

METHODS OF STRAIN ANALYSIS

One of the principal advantages of physical model studies of tectonic deformations is that progressive deformation within the model system can be documented in detail. Similar data obtained from fabric overprinting relationships and measurements of total strain in natural structures can be compared with the experimental data as a means of testing the interpreted kinematic evolution of the natural structures (e.g. Dixon 1975, Platt 1980, Schwerdtner *et al.* 1978, 1983).

Two problems hinder the documentation of strain variation and progressive deformation. First, although some tectonic structures have, or can be idealized as having, cylindrical symmetry (that is, the strain at any point has at least monoclinic symmetry), many structures are truly three-dimensional (the strain at any point may be triclinic). Strain variation in structures of the latter type is difficult to monitor unless the model is constructed with internal three-dimensional strain markers (as has been done by John Morgan, personal communication 1983). We have found that useful semi-quantitative interpretations of three-dimensional strain variation and progressive deformation can be made on the basis of a combination of detailed surface strain data and profile strain data (provided that the structure is close to cylindrical). We describe below two methods by which the resolution of surface and profile strain can be significantly increased. Both of these techniques have been applied in a study of the kinematic evolution of gravity-driven subsided troughs such as synclines between mantled gneiss domes and possibly Archaean greenstone belts (Dixon & Summers 1983).

The second problem is that the models are opaque. Thus in order to monitor the progressive evolution of the structure, either a number of identical models must be deformed to different extents prior to sectioning (e.g. Dixon 1975), or a single model must be sectioned at various stages in its deformation, then carefully reassembled for further deformation. We have had considerable success with the latter approach.

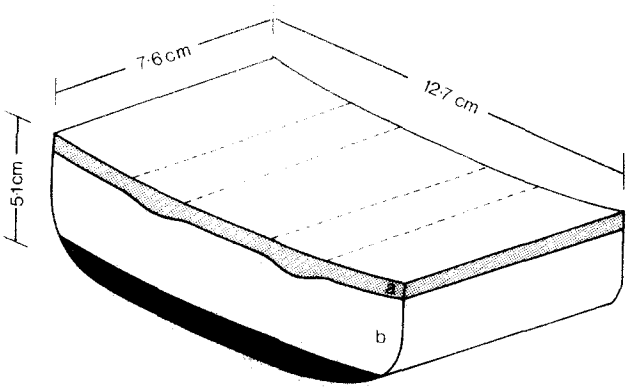

Fig. 3. Schematic drawing of the shape and dimensions of a centrifuge model (this one designed to develop localized subsiding troughs at the sites of thickened surface layer (a)). See text.

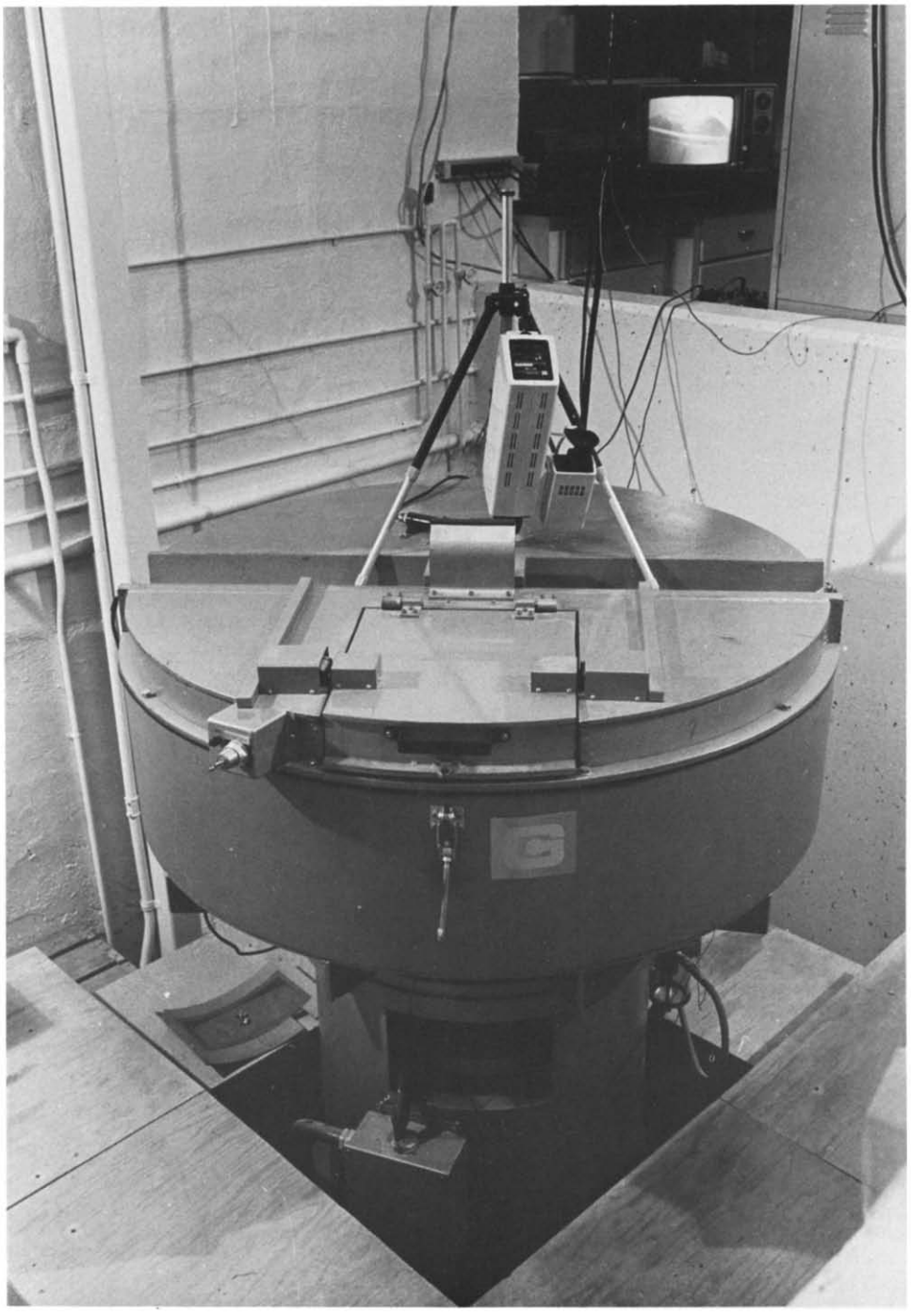

Fig. 1. General view of the 20,000 *g* centrifuge at Queen's University. Note view of model chamber on TV screen (top right).

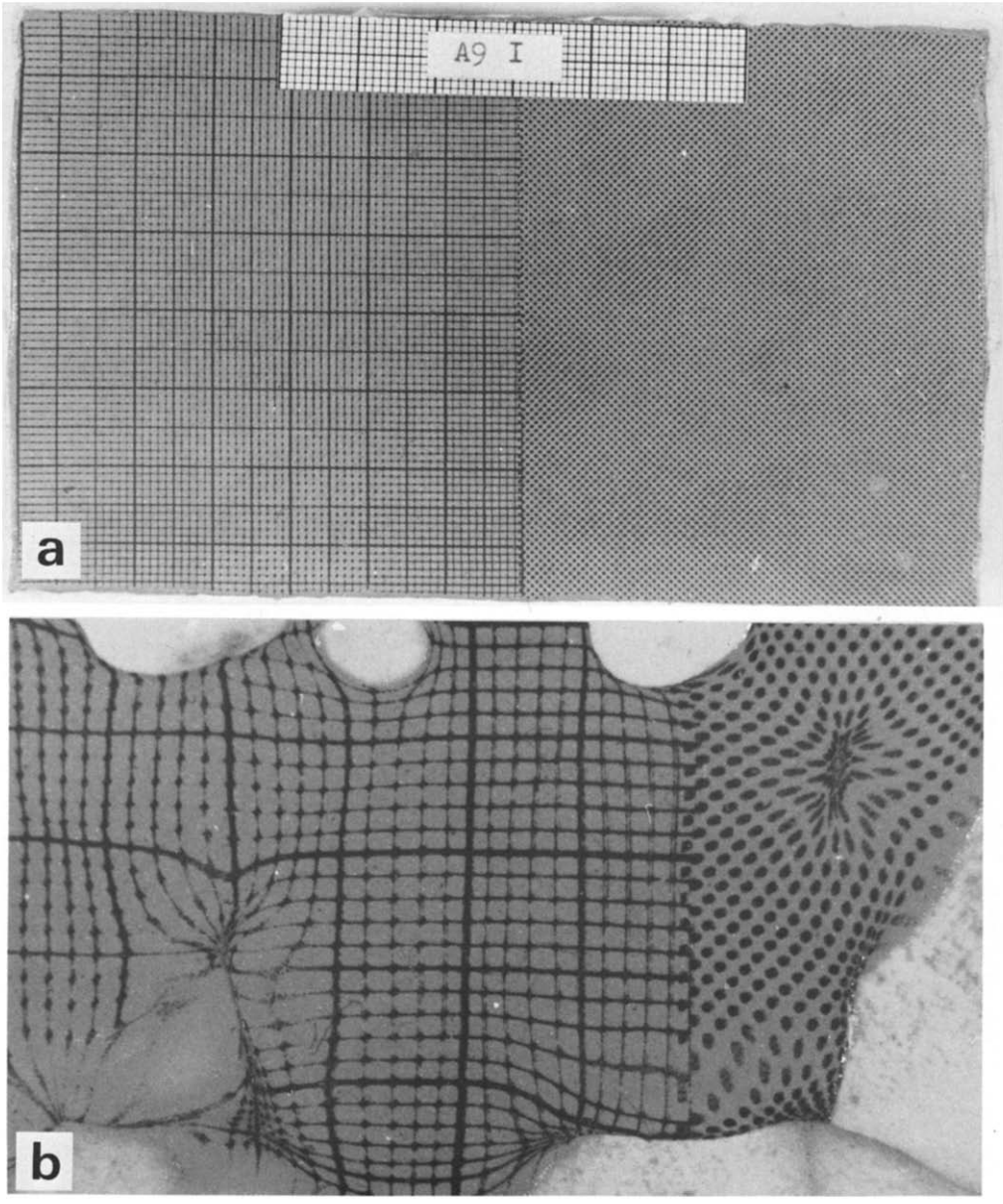

Fig. 4.(a) Undeformed surface strain markers (passive mm-grid and circular dots) transferred to silicone putty surface from a 'soft' graphite print. (b) Enlarged view of a portion of the same model after deformation in the centrifuge produced buoyant rise and spreading of basement diapirs (dilated regions), and subsidence of the dense overburden layer (constricted regions).

Fig. 5. Centrifuge model A18, run a total of 35 mins @ 2000 *g*, developed two parallel, cylindrical troughs in which the relatively dense surface layer subsided into a less-dense basement. (a) and (b) are profile sections illustrating the method of construction (Dixon 1974) whereby, in each half of the model, each tectonic unit is composed of either vertical or horizontal passive colour marker layers in the undeformed state. Superposition of sections from the two halves of the model in the deformed state yields a grid which can be analysed numerically to yield a map of the variation of orientation and relative magnitudes of strain ellipse axes (c) (see text and Dixon & Summers 1983). Scale grids in (a) and (b) are mm squares.

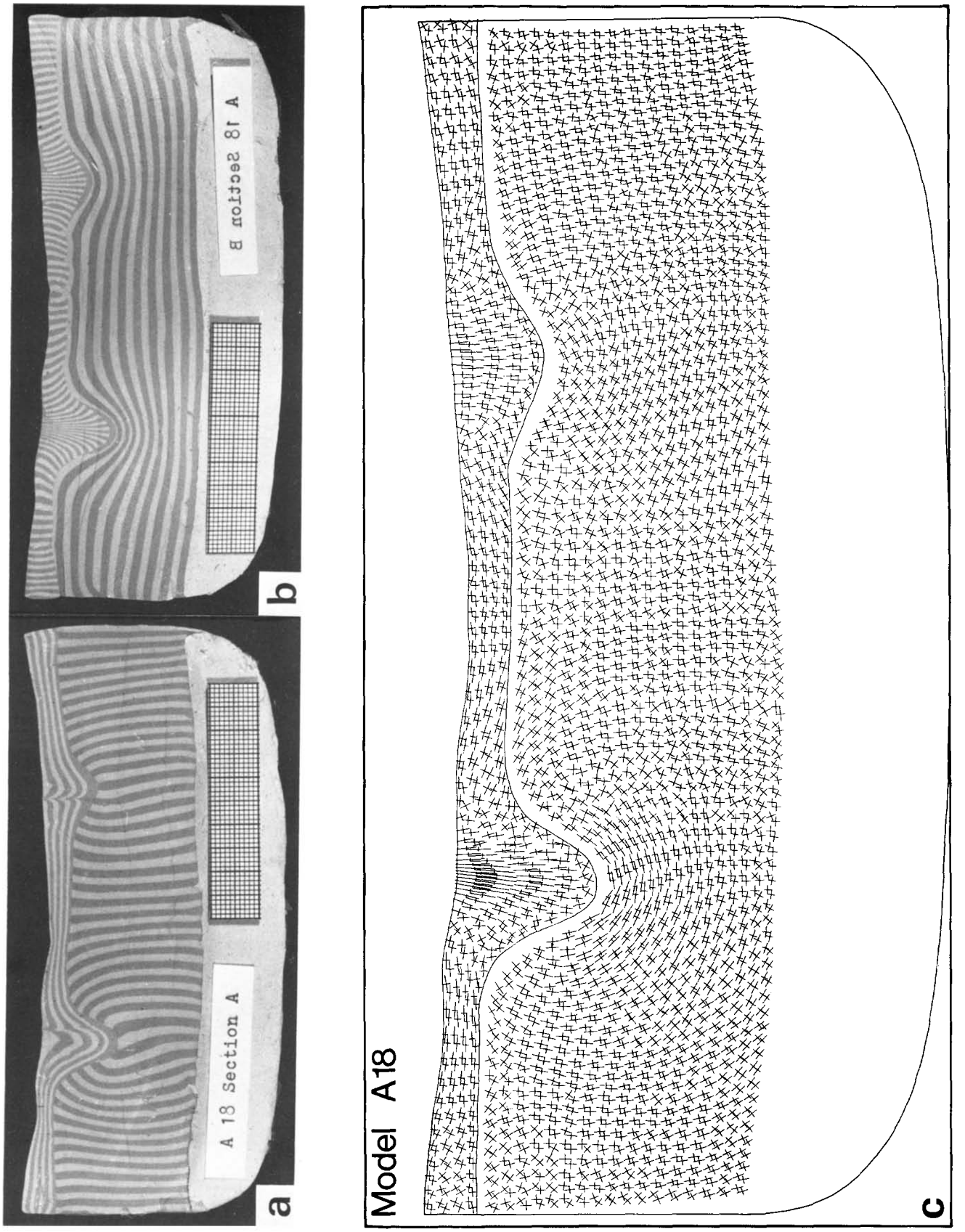
A 18 Section A
a
A 18 Section B
b
Model A18
c

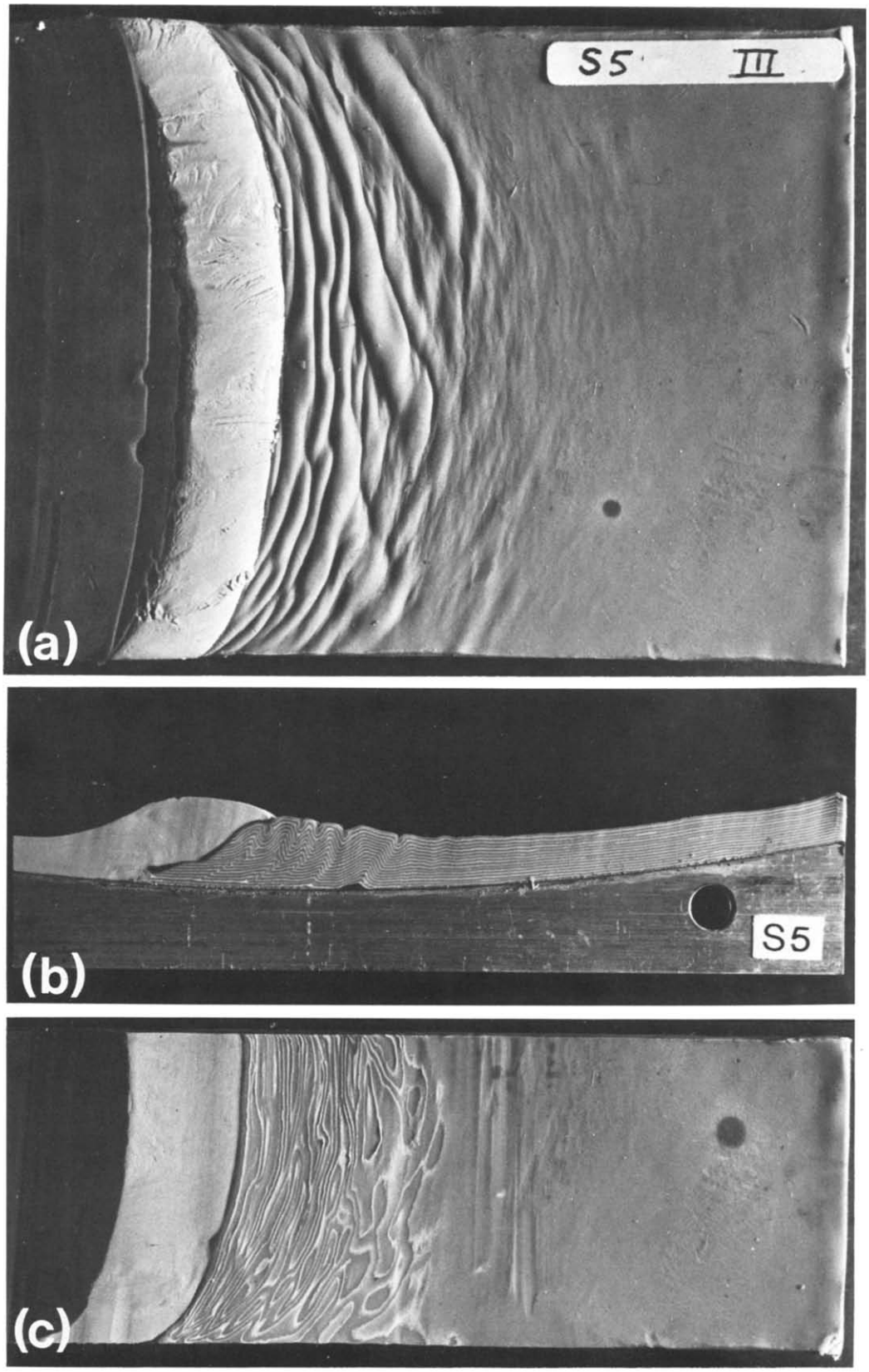

Fig. 6. Model S5 (Sidey 1983) was run in three stages for a total of 55 mins @ 4000 g. A laterally spreading wedge of isotropic material (left side of each photo) has compressed a horizontally layered sequence of competent plasticine and incompetent silicone putty laminae (16 layers of each, all of equal thickness; total thickness 6 mm). The horizontally layered multilayer contained three localized perturbations (anticlines) situated in front of the spreading wedge and oriented at 30° to the wedge front. (a) Plan view of the top surface of the model. Note the interference between the large initial perturbations and the smaller buckle-fold trains that resulted from lateral spreading of the wedge. (b) Vertical cross-section through the centre of the model. Note that the large anticlines at the surface change character at depth and resemble listric thrust discontinuities. (c) Plan view of a horizontal ('erosion') surface cut at a level about $\frac{1}{3}$ of the distance below the top surface of the multilayered sequence. Note the periclinal nature of the folds.

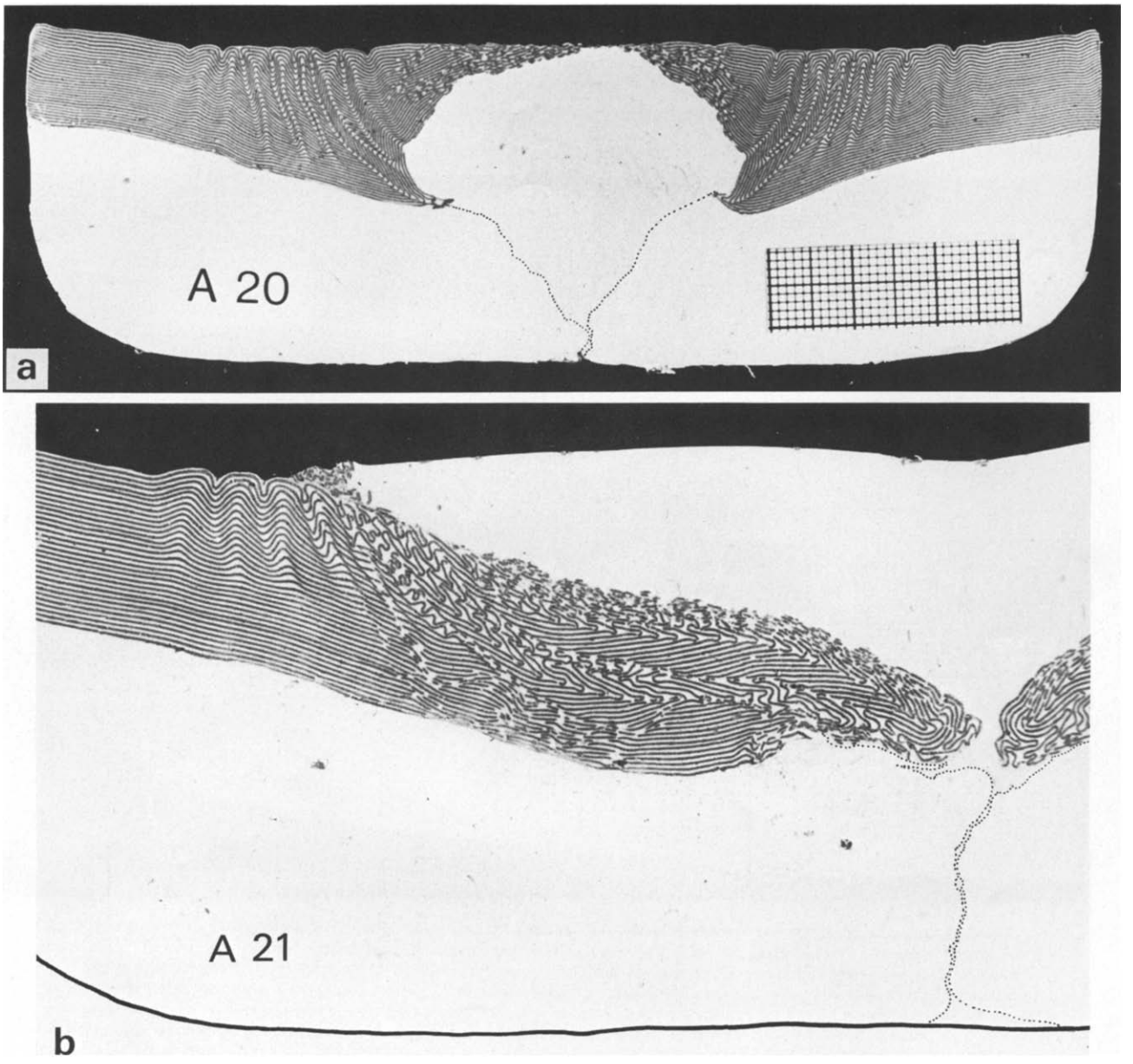

Fig. 7.(a) Profile section of model A20, (run 15 mins @ 2000 ***g*** and 30 mins @ 3000 ***g***), which consisted initially of a horizontally laminated cover sequence (Plasticine/silicone putty; thickness ratio 1:1) that overlay a dense (Plasticine) basement which contained a square (in cross-section) prism of low-density silicone putty. The silicone putty block rose diapirically through the cover sequence, producing horizontal extension (boudinage of Plasticine layers above it and horizontal compression beside it). Note that buckle folds have upright axial surfaces near the surface but that these have been rotated and dip at gentle angles towards the intrusion at depth. Scale grid in mm. (b) Profile section of part of model A21 (run 30 mins @ 2000 ***g***), whose initial configuration was similar to A20 (above) except that the buoyant basement prism had a lower density and lower viscosity. Thus A21 has developed to a more advanced state than A20. Note that progressive overriding of the inclined folds has caused their overturned limbs to be extended and sheared out, while the upright limbs remain as coherent stratigraphic packets.

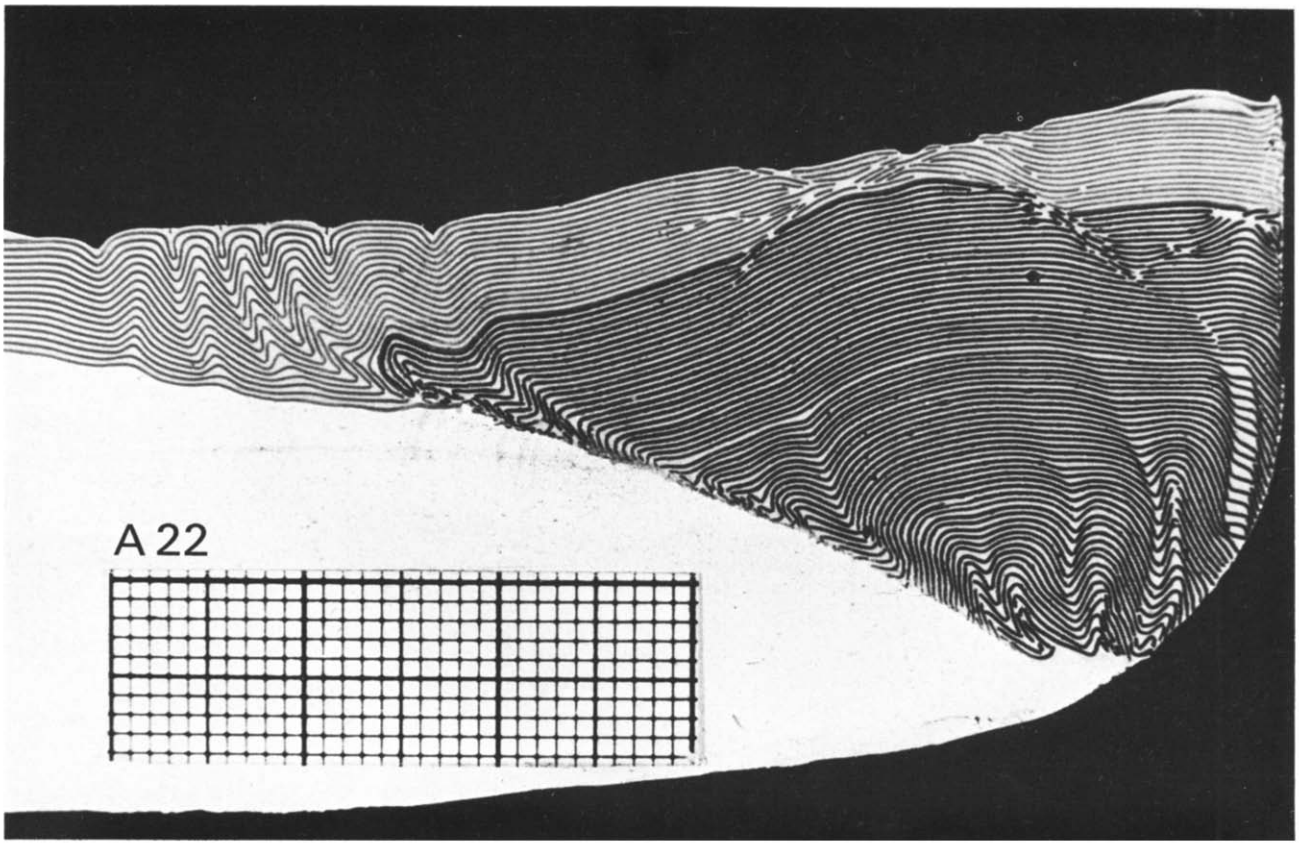

Fig. 8. Vertical profile section of a portion of model A22 (run for 15 mins @ 2000 g and 45 mins @ 3000 g), in which a tapered basement wedge of Plasticine (white area) has spread laterally and caused uplift of the initially horizontally laminated Plasticine/silicone putty multilayer. The upper portions of the uplifted multilayer have undergone layer-parallel extension, with conjugate failure planes propagating at low angles across the layering; gravity sliding of the cover sequence towards the left has produced buckling of the multilayer. The prominent black interface within the thick portion of the multilayer was initially horizontal and level with the top surface of the basement in the left-hand portion of the model. Scale grid in mm.

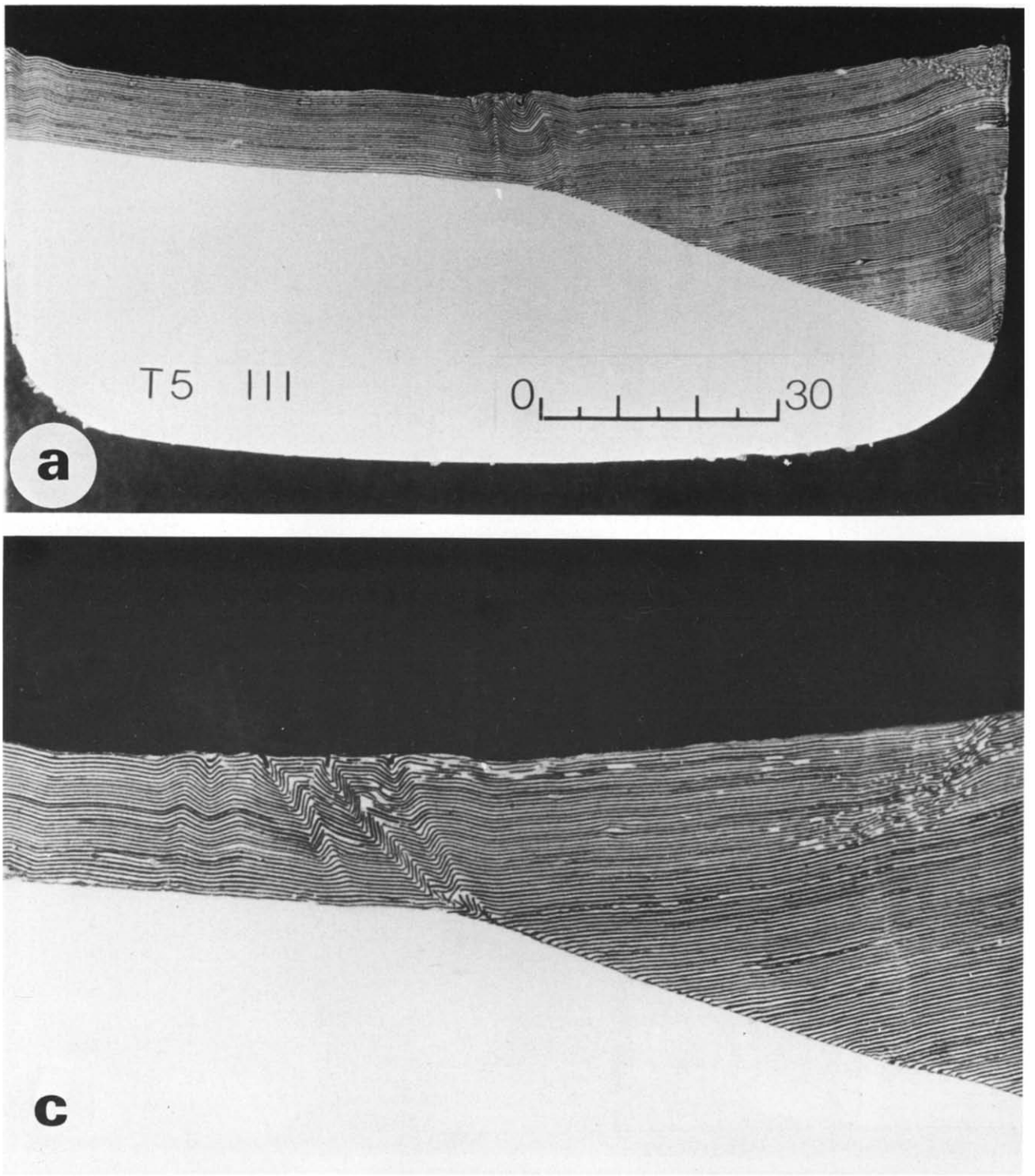

Fig. 13. Centrifuge model T5 consisted initially of a uniformly laminated multilayer of Plasticine and silicone putty (thickness ratio 1:1; each layer 0.156 mm thick; total of 64 layers per cm) 10 mm thick in the left half of the model and tapering to 40 mm thick to the right end, overlying a denser Plasticine substratum (white). During the centrifuge run the Plasticine substrate flowed toward the right, so as to approach a horizontal configuration. As a result the tapered portion of the multilayer was lifted up and its upper portion underwent horizontal extension and gravity gliding towards the left. (a) and (b) illustrate longitudinal profiles through the model after stage III and stage VIII of the experiment; (c) is an enlargement of the central portion of (b); and (d) is the final configuration of the model's top surface (also after stage VIII).

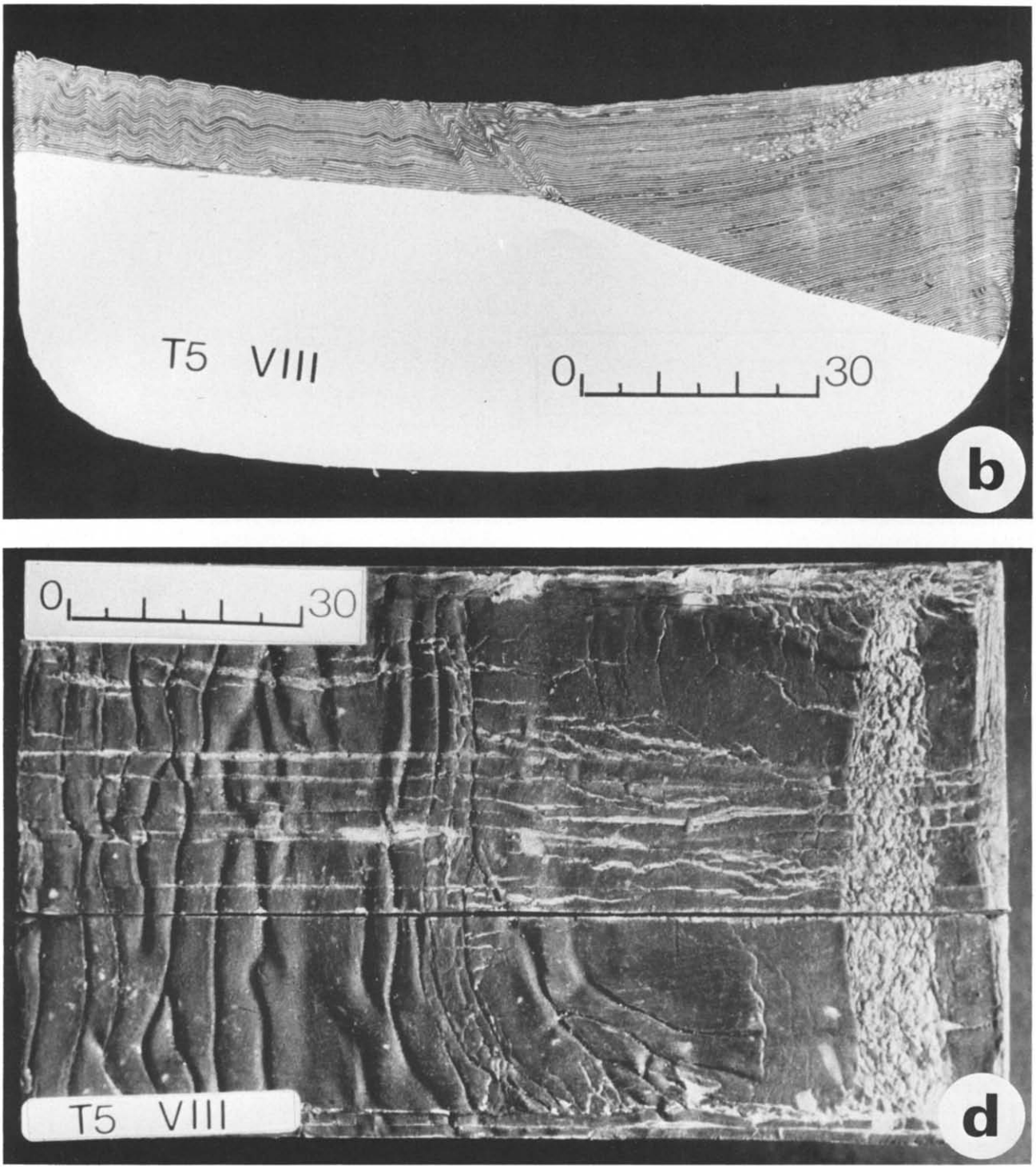

Figure 13—*continued.* Section (b) corresponds with the prominent horizontal line of cut in (d). Note the progressive evolution of the folds in the centre portion of the model, especially the overturning of the axial surfaces. Note also the propagation of low-angle normal faults in the extending portion of the multilayer (upper right corner of a–c). Scale bars labelled in mm. Stage III was reached after 100 mins @ 3000 ***g***. After Stage IV (total of 145 mins @ 3000 ***g***) the acceleration was increased to overcome the decreased gravitational potential in the partially evolved model system. Stage VIII represents 145 mins @ 3000 ***g*** and an additional 110 mins @ 6000 ***g***.

We have run a number of pairs of identical models through as many as ten stages, with one model sectioned along a new profile cut after each stage (see below, Fig. 13) and the other sectioned only at the end of the experiment. The cuts appear to have a minimal effect on the evolution of the structures (provided that they are made transversely to the axis of the overall cylindrical symmetry of the structures). Indeed, in models with anisotropic, finely laminated units, we have observed buckle folds propagate across the section cuts (e.g. in model T5, Fig. 13).

Passive markers for surface deformation

Silicone putty has the particular property of accepting a 'soft' print, such as newsprint, when the print is laid in contact with the putty surface. This property can be exploited by obtaining a loose graphite print (prepared by extracting a photocopy from an electrostatic copier before the final baking stage) of a desired passive marker pattern (e.g. rectangular grid) and imprinting this grid directly on the free, upper surface of a model. The technique allows the imprinting of extremely fine passive grids and resolution of correspondingly fine strain detail. Examples of the use of this method are given in Fig. 4.

The surface grid can be used to document the variation of total and incremental strain and the displacement of nodal points across the top of a model if the model is deformed in stages and photographed at each stage. Furthermore, the total three-dimensional strain and the vertical strain, perpendicular to the model surface, can be calculated at every point if we assume constant volume deformation and that the free surface is a principal plane of the strain ellipsoid at every point. We have applied this method of strain monitoring in our study of the kinematics of trough subsidence (Dixon & Summers 1983).

Passive markers for profile deformation

Deformation within profile sections of cylindrical structures can be monitored using a technique described in detail elsewhere (Dixon 1974, 1975). We report here a means of increasing the resolution of strain determination. The method involves the construction of an individual model in two halves. Within one half, a given unit is constructed with a uniformly spaced horizontal, passive colour banding. In the opposite half, the same unit is constructed with identically spaced passive colour banding in a vertical orientation. The halves are joined, the model deformed and subsequently sectioned along each side of the plane of contact between the two halves so as to reveal deformation of the initially orthogonal passive marker bands (Figs. 5a & b). The deformed patterns are graphically superimposed to generate a deformed grid representing, in effect, profile deformation of an initial field of square elements. The grid is digitized and subjected to computer analysis to define strain variation in the profile plane (Fig. 5c). By using relatively thin marker layers the strain pattern can be revealed in great detail. The profile in Fig. 5c contains strain axes for some 3500 'elements'.

A very finely laminated, passively colour-banded multilayer can be prepared by assembling a stack of layers of equal thickness (e.g. 1–2 mm) but alternating colours, and then reducing the thickness of the whole stack by hand-rolling on a water-wet glass plate. The thinned stack can then be cut, restacked and rolled down again until the desired thickness of individual colour units is attained. In this manner the strain markers can be made small enough that the problems of inhomogeneous strain at the scale of the markers encountered by Dixon (1974, 1975) are avoided. We also improve the resolution by calculating the strain in triangular elements defined by three corners of the initially square markers.

The techniques of strain analysis described above are most applicable to models made up of a small number of relatively thick (neglecting the fine, passive colour banding), isotropic layers. In our work on emplacement of diapirs (Dixon 1975) and trough subsidence (Dixon & Summers 1983) we have used simple, gravitationally unstable layered systems to allow a reasonably controlled interpretation of the deformation pattern in individual models. No attempt was made to incorporate small-scale variations in material properties, simulating rock stratification or other types of initial heterogeneity which might be present in a natural system. This type of modelling is most applicable to the study of large-scale structures that form at relatively deep crustal levels where the effects of rock anisotropy and heterogeneity are reduced.

ACTIVFLY LAYERED MODELS

A contrasting problem is the simulation of the behaviour of stratified sedimentary rock sequences deformed at high crustal levels.

The evolution of large (kilometre) scale structures, particularly fold structures, within horizontally stratified sedimentary sequences has been the subject of a number of published physical model studies (e.g. Willis 1894, Bucher 1956, Blay *et al.* 1977, Dennis & Häll 1978, Guterman 1980). The majority of these experiments were carried out under conditions broadly simulating décollement tectonics. Each of these studies has succeeded in producing model structures with a general geometric similarity to natural large-scale structures. However, application of this work to the interpretation of the progressive evolution of natural structures is limited because of a lack of control on factors influencing experimental deformation. This applies particularly to data on the rheological properties of model materials, clearly a vital consideration in attempts to relate model and large-scale prototype deformation on anything but the most general level. A second consideration in interpreting previous experiments concerns the problem of the geometric scaling of primary structures which are likely to influence natural deformation, or, more specifi-

cally, the problem of scaling natural sedimentary bed thicknesses of the order of metres or decametres. Published experiments involve models incorporating millimetre-scale individual layers which effectively represent prototype bed thicknesses of the order of hundreds of metres. One consequence of this scaling problem is that the bending resistance of discrete layers influences model deformations to a far greater extent than is likely to be the case in natural large-scale prototype processes (e.g. buckle folds, ramp folds, etc.) where slip or shear on incompetent interbeds is a dominant mechanism of bulk deformation.

In designing a programme of centrifuge modelling to study the evolution of large-scale deformation structures in natural sedimentary multilayers, we have set two primary objectives: to develop a construction technique whereby interlayered laminae of contrasting competence, scaling bed thickness of the order of ten metres, can be produced; and to carry out rheological testing of the model materials employed so that meaningful comparisons with prototype materials can be made. We have made significant progress towards both objectives.

A microlaminated, mechanically anisotropic model material composed of alternating layers of the modelling clay, Plasticine (the competent unit), and silicone putty (the incompetent unit) is very easily prepared as follows. Two uniform sheets of Plasticine and silicone putty are rolled out, separately, by hand, on a water-wet glass plate so that the initial ratio of thicknesses of the two sheets is equal to the thickness ratio desired in the final multilayer. Two to five millimetres is a convenient range for the initial thickness of the thinner of the two sheets at this stage. The two sheets are dried, then stacked to produce a two-layer multilayer. The stack is rolled down to the total thickness required for the final multilayer. The combined sheet is then cut, restacked and again rolled down to the final total thickness, giving a four-layer multilayer made up of alternating Plasticine and silicone putty. This process is repeated so that after each stage there is doubling of the total number of laminae and a corresponding reduction in the thickness of individual laminae by a factor of 0.5. The technique, which is akin to that employed by a pastry chef, can achieve remarkably uniform individual laminar thicknesses down to 70 μm in the case of the competent Plasticine, and to 20μm for the incompetent silicone putty. We have constructed multilayers with as many as 128 layers per cm, and with thickness ratios (Plasticine/silicone putty) ranging from 1:1 to 9:1.

The success of the method derives from the particular non-linear rheologies of the two materials. Although they exhibit an effective viscosity contrast of approximately 100:1 at strain rates typically achieved during centrifuge experiments, they appear to have equal viscosities under the higher strain-rate conditions produced by hand-rolling. Thus, the two materials are capable of extending uniformly, without developing a necking instability, under the roller. That the flow curves for the two materials must cross at the rolling stress–strain rate conditions is further demonstrated by an inversion of their competency contrast at higher strain rate: if the multilayer is rolled too fast, the silicone putty develops pinch-and-swell structures relative to the Plasticine. The details of the rheological properties of the Plasticine and silicone putty we have used are discussed below and in Appendix 2.

We have employed the anisotropic microlaminated material in models incorporating a range of relatively simple, geologically representative stress and displacement boundary conditions, such as (a) compression of horizontally-stratified sequences under 'thin-skinned' or 'décollement' conditions (Fig. 6); (b) localized basement uplift leading to gravity glide of a stratified cover (Fig. 7); (c) gravitational spreading of a stratified wedge (Fig. 8) and (d) subsidence of relatively dense stratified supracrustal sequences and buoyant rise of adjacent diapiric basement domes (Dixon & Summers 1983).

RHEOLOGICAL PROPERTIES OF THE MODEL MATERIALS

We have performed a series of rheological tests on the particular grade of silicone putty (designed SP4 in our lab.) that we use in constructing the laminate described above. This putty was obtained from Binney & Smith (Canada) Ltd. as their Silicone Putty no. 101, but it is manufactured by the Dow-Corning Chemical Company as Dilatent Compound no. 3179. We have also attempted to assess the rheological properties of our Plasticine, which is Harbutt Gold Medal brand, in terms of the data for Harbutt Standard White Plasticine given by McClay (1976) and results of simple tests performed in our lab. We have not performed a full series of tests on our Plasticine, as our test rig in its present form is not designed for the stress levels that would be required. The test rig and the method of data analysis are described in Appendix 1, and details of the rheological properties of silicone putty and Plasticine are given in Appendix 2.

Before summarizing the results of our rheological tests, we would like to emphasize that there is likely to be considerable variation in the physical properties of the materials obtained from different suppliers, and even of different batches of a material from one supplier. Thus, differences in results of tests by various workers are not solely due to differences in precision or test method. As scale modelling becomes more sophisticated, rheological tests will have to be done on a routine basis, perhaps on each batch of model material used.

Properties of silicone putty

An example of a series of constant-load creep curves for silicone putty SP4 is shown in Fig. 9. The material does not exhibit a well-defined instantaneous elastic response to the application of a load in these tests, although of course it is rather elastic in a 'bounce' test. The material does exhibit significant primary creep which is recoverable on unloading. Total recoverable elastic strain is related to applied stress as shown in

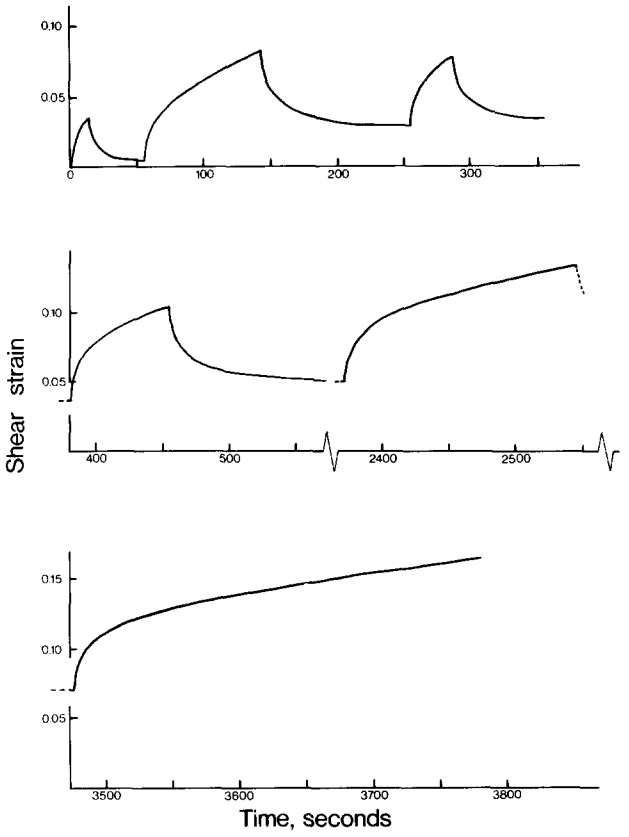

Fig. 9. Creep and relaxation behaviour of silicone putty SP4 shown by variation in shear strain ($\hat{e}_{rz}$) with time. The test involved loading of the silicone putty in the annulus and subsequent relaxation by removing the load for progressively increasing periods of time. Temperature = 18°C; (calculated) shear stress, σ_{rz}, at the mid-point of the annulus = 4.0×10^2 Pa.

Fig. 10. This dependence corresponds to a rigidity modulus for total elastic strain of 10 kPa.

Creep curves such as shown in Fig. 9 have been analysed to define 'bulk' strain rate $\hat{\dot{e}}$ (where $\hat{}$ indicates quantity averaged over the full width of the test annulus, rather than measured at a particular radial position) at a 'bulk' shear strain of 0.2. These data are plotted against applied shear stress (at the mid-point of the annulus) for

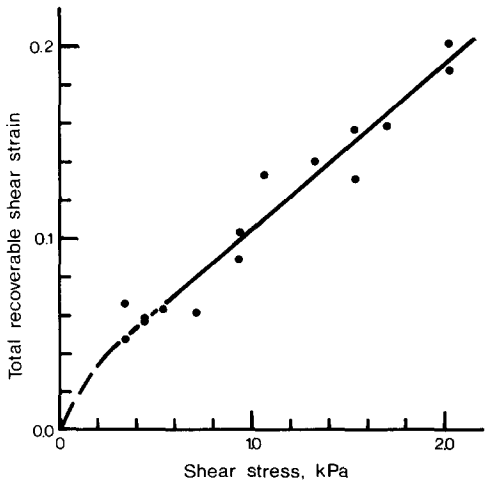

Fig. 10. Plot of total recoverable shear strain vs (calculated) applied shear stress, obtained from a series of tests on silicone putty SP4 (see text and Appendix 2).

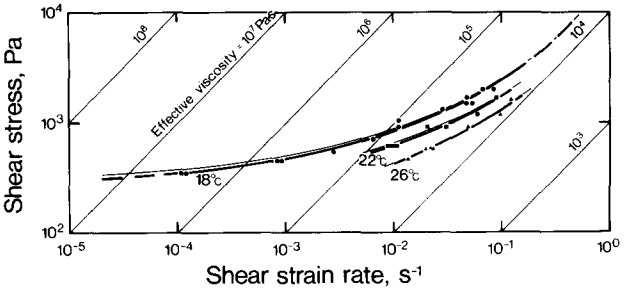

Fig. 11. Summary of test results on silicone putty SP4 obtained at 18 ± 1°C (dots), 22 ± 1°C (squares) and 26 ± 1°C (triangles). Heavy curves were fitted (by eye) to the data at each temperature. Light curves are adjusted to take account of the radial stress gradient across the test annulus (see text and Appendix 2 for discussion), and represent the variation of local shear strain rate with shear stress at the radial mid-point of the annulus (i.e. at $r = (r_0+r_1)/2$).

tests at three temperatures in Fig. 11, and the curves through the test data have been shifted to convert 'bulk' strain rate to true 'local' strain rate at the annulus mid-point (fine lines on Fig. 11; see Appendix 2 for more detailed discussion).

The silicone putty exhibits creep behaviour that is neither linear (unit slope on the log–log plot of Fig. 11) nor power-law (data points on a line of constant slope = $1/n$). Rather, its behaviour approximates to power-law with $n = 7 \pm 2$ at strain rates in the range 10^{-5}–10^{-3} s^{-1}, with an apparent decrease of the value of n towards higher strain rates. It exhibits a yield strength of about 300 Pa in very long-term experiments (strain rates lower than 10^{-7} s^{-1}), and is interpreted to tend towards linear behaviour at higher strain rates on the basis of convergence with the flow strength of Plasticine during multilayer rolling (see above and Appendix 2).

Properties of Plasticine

McClay (1976) reported results of constant strain-rate, pure shear tests on three grades of Harbutts Plasticine, one of which (Standard White) closely resembles the Gold Medal brand used by us. At strain rates between 10^{-6} and 10^{-3} s^{-1} and 25°C, this material exhibits power-law behaviour with $n = 6$–9. We assume that this flow law is correct, but on the basis of several lines of evidence we suspect that our Plasticine is approximately one order of magnitude weaker than McClay's results for Standard White (see Appendix 2). On Fig. 12 we show McClay's stress–strain rate curve for Standard White Plasticine (labelled P), our preferred curve for Gold Medal Plasticine (P′), and the shifted curves for silicone putty SP4 from Fig. 11.

MODEL SCALING

In order to consider the validity of the use of model multilayers as analogues for the behaviour of natural stratified rock systems we will use the experiment illustrated in Fig. 13 as a basis for discussion. Emphasis will be placed on mechanical properties of the model mul-

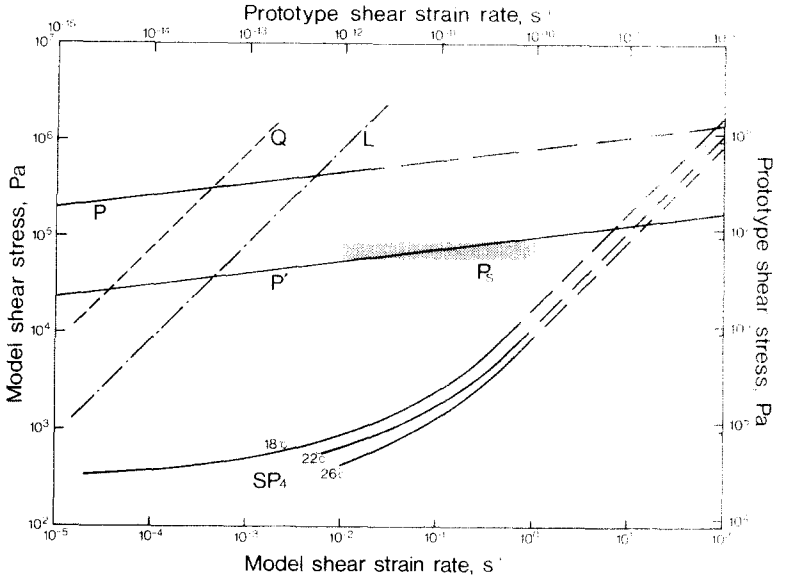

Fig. 12. Shear stress vs shear strain rate plot illustrating the rheological behaviour of model materials and selected natural rocks. The left-hand ordinate and lower abscissa refer to model materials, and the right-hand ordinate and upper abscissa to the natural prototypes, using scale ratios discussed in the text and Table 1. The three curves labelled SP4 are the adjusted curves for silicone putty, taken from Fig. 11. P represents data for Harbutt's Standard White Plasticine (McClay 1976), including extrapolation to high strain rate (dashed portion of curve). P' is our preferred curve for the behaviour of the similar Harbutt's Gold Medal Plasticine, based on results of slope failure experiments (shaded region, P_S (Stevens 1983)) and other arguments (see text and Appendix 2). Q and L are calculated from theoretical flow laws for quartzite and limestone (Rutter 1976), deforming by pressure solution at 100°C (100 μm grain-size).

tilayers. We use scaling relationships to define the properties of large-scale prototype systems represented in the model and then we consider how closely these properties may match known characteristics of natural systems (see Table 1).

The intitial configuration of model T5 can be visualized from Fig. 13(a), which is a longitudinal profile of the model at a relatively early stage (III) of the deformation. The model is made up of an isotropic 'basement' constructed from Gold Medal Plasticine, overlain by a stratified Plasticine–silicone putty multilayer. One end of this multilayer is thickened to form a wedge which tapers out into a plate with uniform thickness. The top and base of this section of the multilayer are initially parallel to equipotential surfaces of the centrifugal force field and represent horizontal surfaces in the earth's gravitational field. The configuration involves an initial unstable density distribution such that the wedge section of the multilayer undergoes uplift and lateral spreading (Figs. 13 a–c) during the course of the experiment. This process results in the sequential development of folds in front of the zone of lateral spreading and also in the development of structures representing the response of the multilayer to layer-parallel extension in the region overlying the core of the uplifted wedge (Fig. 13c). The problem we consider here is whether observation of the progressive evolution of individual fold structures and extensional structures can be used, even in general terms, to gain an understanding of the behaviour of a stratified sedimentary system deformed in a large-scale tectonic framework which is broadly equivalent to that of the model.

An essential feature of centrifuge model experiments is that they are designed to represent prototype processes occurring on a scale sufficiently large that work associated with change in gravitational potential of the prototype is a significant component of the total work spectrum of the deforming prototype system. Any model simulating such a process is subject to scaling conditions of the type described, in a geological context, by Hubbert (1937) and Ramberg (1967). Rather than repeat the clear discussions given by these authors we will simply use quantitative scale relationships which they obtain from arguments which involve a consideration of the need to scale the relative contributions of gravitational work and work associated with the development of internal strain fields within the model and the prototype systems. The reader is referred to Hubbert's and Ramberg's works for a complete derivation of the relationships used and an explanation of their physical significance. There is, however, a need to re-emphasize that the equations are derived on the assumption that scaling of gravitational work is critical to the simulation. The authors are aware of cases in the literature and in a number of unpublished theses where the Hubbert–Ramberg equations are used to analyse model simulations of small-scale tectonic processes in which gravitational work represents a negligible proportion of the total deformation work of the system. Application of the Hubbert–Ramberg equations to such models leads to totally unnecessary restrictions in discussions of the nature of similitude between model and prototypes and would suggest a lack of understanding of the basis on which the scaling equations used are derived.

The rheological properties of prototype materials whose behaviour is simulated at reduced scale and under increased deformation rates in centrifuge experiments can be most conveniently defined on the basis of four model ratios:

l_r, the ratio between equivalent lengths in the model and prototype. In simulations of the type illustrated in Fig. 13 this ratio lies in the range 10^{-5}–10^{-6}. For the purpose of this discussion we use $l_r = 5 \times 10^{-6}$ (10 mm in model = 2 km in prototype).

ρ_r, the ratio between densities of equivalent material elements in model and prototype. Here $\rho_r = 0.6$, as the bulk density of the model multilayer is 1.45 g cm^{-3} and the bulk density of the prototype sedimentary stack is assumed to be 2.4 g cm^{-3}.

a_r, the ratio between the centrifugal acceleration (under which a given experiment is run) and Earth's gravitational acceleration, typically 2×10^3–7.5×10^3. For the purposes of this discussion we use $a_r = 4 \times 10^3$.

t_r, the ratio between times of equivalent deformation events in model and prototype. This parameter is loosely constrained by a knowledge of model deformation rates and likely prototype deformation rates. Here we choose $t_r = 10^{-10}$ (1 hour model time = 1.15 Ma prototype).

Given these parameters, specific aspects of the rheological behaviour of the model materials can be scaled so as to define equivalent properties of prototype materials whose behaviour is simulated in specific experiments. These scaled properties will be considered in the light of information available on various natural sedimentary rock types. The comparison allows one to judge the extent to which observations on the evolution of model structures can be extrapolated to natural structures.

Elastic properties

Silicone putty did not exhibit any marked instantaneous elastic strain at the relatively low stress levels employed in our tests (e.g. the creep curves of Fig. 9). We can, however, derive a 'total' elastic rigidity modulus, from the slope of the total recoverable elastic strain vs stress plot of Fig. 10. We obtain a value of $G_{\text{total}} = 5.5$ kPa from the low-stress end of this curve.

The model ratios stated above may be combined to yield a model ratio for stress of

$$\sigma_r = \frac{\sigma_{\text{model}}}{\sigma_{\text{prototype}}} = l_r\, \rho_r\, a_r = 0.012.$$

Thus the 'total' rigidity modulus for silicone putty corresponds to a prototype 'total' rigidity modulus of 4.6×10^2 kPa. If we assume that the 'total' elastic strain is approximately 4–5 times the instantaneous, then the prototype modulus of rigidity for instantaneous elastic strain is ~2 MPa.

Creep properties

The most convenient way to define the scaled flow behaviour of prototype multilayer components represented by Plasticine and by silicone putty is to rescale the log stress and log strain rate axes of Fig. 12 according to the chosen model ratios listed previously. Data lines for Plasticine and silicone putty behaviour are directly transformed to equivalent representations of the flow behaviour of the competent and incompetent prototype multilayer components by this rescaling.

The following properties characterize the behaviour of these prototype components. (a) Over a 'geologically representative' range of prototype strain rates (10^{-14} s^{-1}–10^{-12} s^{-1}), both competent and incompetent prototype multilayer components show a highly non-linear relationship between shear strain rate and shear stress. A strain rate of 10^{-16} s^{-1} can be taken as negligible, for any practical purpose, and if the shear stress level at this rate of strain is taken as an effective yield strength then the competent unit displays a yield strength of 1.25 (curve P')–12.5 (curve P) MPa. (b) The ratio of 'competence' or flow strength between the two components is 67 (P')–667 (P) for a shear strain rate of 10^{-13} s^{-1}. The prototype multilayer is highly anisotropic and fold development in this system can be expected to be dominated by shear within incompetent strata, as is obviously so in the centrifuge models (e.g. Fig. 13c).

RELATIONSHIP BETWEEN SCALED PROTOTYPE PROPERTIES AND PROPERTIES OF NATURAL SEDIMENTARY ROCK MATERIALS

We now consider the extent to which the prototype multilayer properties described may match equivalent properties known for natural sedimentary rock materials. It is clear that, for the chosen scale ratios, the models simulate deformation of a prototype system incorporating strong (indurate) competent layers and relatively weak interbeds. As an example of a natural sedimentary sequence with these general characteristics, we will take a uniform stack of alternating indurate limestones and shales. Experimental and theoretical data on the rheology of limestones are available from a number of sources. Equivalent properties for 'shale' are more difficult to define.

Table 1 lists the values of a series of geometric and mechanical parameters which are likely to play a significant role in influencing deformation of the type of system modelled in experiment T5. The parameters are defined for (a) the centrifuge model; (b) a large-scale prototype system scaled from the model using the model ratios listed previously and (c) a geometrically idealized natural sedimentary multilayer made up of alternating indurate limestone and shale interbeds.

Of main interest in this discussion is the degree of correspondence between mechanical properties of the hypothetical scaled prototype multilayer and equivalent properties of a limestone–shale sedimentary multilayer.

Table 1. Geometrical and mechanical parameters for centrifuge model T5, a prototype scaled from the model, and an idealized sedimentary multilayer

	Model multilayer		Model ratio	Prototype multilayer (scaled from model)		Limestone–shale multilayer	
Total thickness	10 mm		$l_r = 5 \times 10^{-6}$	2 km		1.5–5 km	
Thickness ratio (competent: incompetent layers)	1:1		—	1:1		variable	
Mean fold wavelength at surface	8 mm		$l_r = 5 \times 10^{-6}$	1.6 km		variable	
Mean density	1.45 g cm^{-3}		$\rho_r = 0.6$	2.4 g cm^{-3}		variable	
Centrifugal (gravitational) acceleration	4000 g (c.g.)		$a_r = 4 \times 10^3$	1 g		1 g	
Strain rates (estimated) during fold amplification	$<5 \times 10^{-12}$ s^{-1}*		$t_r = 10^{-10}$	$<5 \times 10^{-12}$ s^{-1}		?$<10^{-12}$ s^{-1}†	
	Comp. unit	Incomp. unit		Comp. unit	Incomp. unit	Limestone	Shale
Layer thickness	0.156 mm	0.156 mm	$l_r = 5 \times 10^{-6}$	31.2 m	31.2 m	variable	variable
Elastic rigidity modulus	NA	$\sim 4.6 \times 10^2$ kPa	—	NA	~2 MPa	20–30 GPa‡	NA
Total recoverable elastic strain§	NA ?<0.01	<0.01	$e_r = 1$	NA ?<0.01	<0.01	NA	NA
Nature of flow law governing creep	non-linear (power law) $6 < n < 9$	non-linear (pseudo-plastic)		non-linear (power law) $6 < n < 9$	non-linear (pseudo-plastic)	linear‖ non-linear¶ (?power law) ?$n > 3$	NA
"Yield strength"**	15–150 kPa	0.3 kPa	$\sigma_r = 1.2 \times 10^{-3}$	1.25–12.5 MPa	25 MPa	8.5 kPa‖ 10–100 MPa¶	NA
Stress at strain rate of 10^{-13} s^{-1} (prototype) 10^{-3} s^{-1} (model)	30–300 kPa	0.45 kPa	$\sigma_r = 1.2 \times 10^{-3}$	2.5–25 MPa	37 kPa	8.5 MPa‖ 10–100 MPa¶	NA
Effective viscosity contrast††	67–667			67–667		NA	

*Estimated from observed growth rates of experimental folds assuming flexural flow in incompetent silicone putty.
†See Price (1975); Pfiffner & Ramsay (1982).
‡See Turcotte & Schubert (1982).
§Estimated for a model strain rate of 10^{-3} s^{-1} and equivalent scaled prototype strain rate of 10^{-13} s^{-1} ($t_r = 10^{-10}$).
‖Pressure solution deformation mechanism (Rutter 1976), 100 μm grain size calcite aggregate, 100°C.
¶Estimates for deformation by twinning on calcite *e* twins in calcite grain aggregate at 10^{-13} s^{-1}, 100°C. Precise data unavailable as rate-controlling factors such as grain solution and translation gliding may contribute to maintenance of grain-to-grain strain compatibility at 'geological deformation rates' (Tullis 1980).
**"Yield strength" defined as stress at 10^{-9} s^{-1} (model) and 10^{-16} s^{-1} (prototype) strain rates.
††Calculated for strain rates of 10^{-3} s^{-1} (model) and 10^{-13} s^{-1} (prototype).
NA, data not available.

The sources of data for limestone are noted in the table. In estimating the various mechanical characteristics listed we have assumed the natural deformation conditions of interest to be temperatures in the range 0–100°C, lithostatic pressures in the range 0–50 MPa and strain rates ranging up to 10^{-12} s^{-1}. These conditions broadly correspond to those simulated in the zone of model T5 in which décollement folds develop. Clearly the scaled prototype parameters listed in Table 1 are valid only for the chosen model ratios and could be changed by introducing different ratios into the scaling equations (e.g. taking l_r as 2×10^{-6} would (a) increase prototype stress levels, strengths and viscosities by a factor of 2.5 and (b) increase the scale prototype multilayer thickness to 5 km and the individual bed thickness to 78 m.)

In estimating properties of limestone we have considered, separately, two mechanisms which are likely to contribute to creep in this material in high level crustal environments—pressure solution and deformation by twinning. Pressure solution data are based on Rutter's (1976) theoretical analysis of factors controlling creep rates associated with this intercrystalline mechanism. Estimates for mechanical twinning are based on a review by Tullis (1980) and experimental and theoretical studies of this mechanism in calcite single crystals and in limestones by Griggs *et al.* (1951, 1953, 1960) and Turner *et al.* (1954).

The following points are brought out in Table 1.

(i) The scaled prototype bed thickness is 31 m. Even though this represents a significant improvement on the massive thickness simulated in previous models of décollement folding, this dimension is still large in terms of likely effective bed thickness in a natural sedimentary sequence incorporating limestone units.

(ii) Comparison of elastic rigidity moduli for prototype units and natural analogue is hindered by lack of data for Plasticine and shale. Limestone with a rigidity modulus of 20–30 GPa (Turcotte & Schubert 1982), should be represented by a model material with a modulus of 240–360 MPa. While data for Plasticine are unavailable, this material is unlikely to be so stiff. Our data for silicone putty suggest that at low stress levels it is a suitable elastic analogue for 'shales' if these have a modulus of ~2 MPa. We have found no estimate for the

elastic modulus of 'shales', relevant to natural deformation conditions, but suspect that they are rather stiffer! (Turcotte & Schubert (1982) quote a value of 14 GPa for shale, but give no details of water content or degree of induration.) Thus the two model materials employed have moduli that are probably too low. However, as the elastic strains produced at model creep stresses are very low (<1%), and the contribution of elastic strain to model deformation is thus relatively small, this scaling problem is not likely to be significant.

(iii) Scaled differential stress levels are of the order of 2.5–25 MPa within the competent multilayer component at a scaled strain rate of $10^{-13}\,s^{-1}$. In general terms, this level of stress corresponds reasonably well with various published estimates of tectonic stresses operating within indurate limestones at geological strain rates in the range $10^{-14}\,s^{-1}$ to $10^{-12}\,s^{-1}$. If the lower part of this range is taken as most representative of scaled Plasticine flow properties then the scaled differential stress level would accord well with the pressure solution data at strain rates of the order $10^{-14}\,s^{-1}$ to $10^{-13}\,s^{-1}$, but would be too low (by an order of magnitude) to simulate stress levels at which significant twinning strains would develop.

(iv) Both competent and incompetent model multilayer components and, therefore, their scaled prototype equivalents show a highly non-linear (approximately plastic) relationship between strain rate and stress at deformation rates generated during folding. This type of behaviour would correlate, in general terms, with deformation characteristics of limestones undergoing creep through twinning and translation gliding. The plasticity of the competent unit would not represent an accurate simulation of the linear flow relationship associated with pressure solution.

(v) It is difficult to make specific comments on the degree of similarity between the flow properties of the scaled incompetent units and those of, for example, shales within a natural multilayer. There is very little information in the literature on the flow characteristics of this material although, clearly, shale properties are critically dependent on the related factors of the pore fluid content, fluid pressure and degree of induration. However, the low strength computed for the scaled incompetent unit means that the simulation is valid only where the strength of the natural shale interbeds is significantly lower than that of the adjacent competent strata. This would be the case where the shales retain sufficient fluid content and pressures to flow under low differential stresses of the order 50–800 kPa representative of scaled prototype differential stress levels at 'tectonic' strain rates.

CONCLUSIONS

The advances in equipment, model construction techniques and knowledge of rheological properties of model materials reported here, and the scaling relationships discussed, will, we hope, lead to an increase in confidence in the validity of analogue modelling of tectonic processes.

This work represents the first stage in an experimental program which is focused on the nucleation and propagation of folds and thrust faults. The microlaminated model material readily forms ductile fold structures (see Figs. 6, 7, 8, 13), and our analysis of relevant scaling relationships has demonstrated that it is a remarkably good analogue for interbedded limestone–shale sequences undergoing ductile deformation at high crustal levels.

The material responds to layer-parallel extension by failing on conjugate shear surfaces that comprise localized necking failure of the competent Plasticine layers and ductile shear of the incompetent silicone putty (see Figs. 7, 8, 13). This mode of failure results in an anastomosing network of shear surfaces which surround relatively undeformed packets of the multilayer, the whole resembling at a large scale a network of normal faults, or at a smaller scale a disrupted tectonic mélange.

In some circumstances of layer-parallel compression the multilayered material can develop shear offsets which resemble listric thrust faults that terminate upwards in fold cores (see Fig. 6b). There remains a need to develop a model material that is capable of developing brittle shear fractures under layer-parallel compression while still fulfilling the other requirements for dynamic similitude.

Although we have made some progress towards characterization of the rheological properties of the silicone putty and Plasticine that we commonly use, more complete testing is still required. The properties of the materials are very sensitive to temperature, and may also be affected by confining pressure (which could be as high as 6 MPa at the base of a model during a typical experiment run at 7500 g). We must also bear in mind the potential for variability among materials of different manufacture, and re-emphasize the need for routine rheological testing accompanying all quantitative model studies.

Acknowledgements—The programme of experimental tectonic modelling at Queen's, of which this effort is a part, has received financial support from the Natural Sciences and Engineering Research Council of Canada through operating grant A9146 and equipment grant E4046 to JMD, and a University Research Fellowship and grant U0140 to JMS; from the Ontario Geological Survey through O.G.R.F. grant No. 68 to JMD; and from the Queen's University Advisory Research Committee (grants to JMD). This financial support is gratefully acknowledged. The Department of Computing Services at Queen's is acknowledged for providing access to computational facilities.

We thank Christopher Peck for assistance with the photography, and Jewel Jeffrey and Linda Harris for typing the manuscript.

The constructive criticisms offered by two anonymous referees resulted in significant improvement of the manuscript.

REFERENCES

Blay, P., Cosgrove, J. W. & Summers, J. M. 1977. An experimental study of the development of structures in multilayers under the influence of gravity. *J. geol. Soc. Lond.* **133**, 329–342.

Bucher, W. H. 1956. Role of gravity in orogenesis. *Bull. geol. Soc. Am.* **67**, 1295–1318.

Cobbold, P. R. 1975. A biaxial press for model deformation and rheological tests. *Tectonophysics* **26**, T1–T5.

Dennis, J. G. & Häll, R. 1978. Jura-type platform folds: a centrifuge experiment. *Tectonophysics* **45**, T15–T25.
Dixon, J. M. 1974. A new method for the determination of finite strain in models of geological structures. *Tectonophysics* **24**, 99–114.
Dixon, J. M. 1975. Finite strain and progressive deformation in models of diapiric structures. *Tectonophysics* **28**, 89–124.
Dixon, J. M. & Summers, J. M. 1983. Patterns of total and incremental strain in subsiding troughs: experimental centrifuge models of inter-diapir synclines. *Can. J. Earth. Sci.* **20**, 1843–1861.
Griggs, D. T., Turner, F. J., Borg, I. & Sosoka, J. 1951. Deformation of Yule marble—IV. Effects at 150°C. *Bull. geol. Soc. Am.* **62**, 1385–1406.
Griggs, D. T., Turner, F. J., Borg, I. & Sosoka, J. 1953. Deformation of Yule marble—V. Effects at 300°C. *Bull. geol. Soc. Am.* **64**, 1327–1342.
Griggs, D. T., Turner, F. J. & Heard, H. C. 1960. Deformation of rocks at 500 to 800°C. In: *Rock Deformation* (edited by Griggs, D. T. & Handin, J.). *Mem. geol. Soc. Am.* **79**, 56–61.
Guterman, V. G. 1980. Model studies of gravitational gliding tectonics. *Tectonophysics* **65**, 111–126.
Hubbert, M. K. 1937. Theory of scale models as applied to the study of geological structures. *Bull. geol. Soc. Am.* **48**, 1459.
McClay, K. R. 1976. The rheology of plasticine. *Tectonophysics* **33**, T7–T15.
Pfiffner, O. A. & Ramsay, J. G. 1982. Constraints on geological strain rates: arguments from finite strain states of naturally deformed rocks. *J. geophys. Res.* **87**, 311–321.
Platt, J. P. 1980. Archaean greenstone belts: a structural test of tectonic hypotheses. *Tectonophysics* **65**, 127–150.
Price, N. J. 1975. Rates of deformation. *J. geol. Soc. Lond.* **131**, 553–575.
Ramberg, H. 1967. *Gravity, Deformation and the Earth's Crust*. Academic Press, London.
Rutter, E. H. 1976. The kinetics of rock deformation by pressure solution. *Phil. Trans. R. Soc.* **A283**, 203–219.
Schwerdtner, W. M., Stott, G. M. & Sutcliffe, R. H. 1983. Strain patterns of crescentic granitoid plutons in the Archean greenstone terrain of Ontario. *J. Struct. Geol.* **5**, 419–430.
Schwerdtner, W. M., Sutcliffe, R. H. & Troëng, B. 1978. Patterns of total strain within the crestal region of immature diapirs. *Can. J. Earth Sci.* **15**, 1437–1447.
Sidey, J. A. 1983. A centrifuge model study of the interaction of two separate folding events. Unpublished B.Sc. thesis, Queen's University, Ontario.
Stevens, T. A. C. 1983. A centrifuge study of slope stability using plasticine. Unpublished B.Sc. thesis, Queen's University, Ontario.
Terzaghi, K. & Peck, R. B. 1967. *Soil Mechanics in Engineering Practice*, Second Edition. Wiley, New York.
Tullis, T. E. 1980. The use of mechanical twinning in minerals as a measure of shear stress magnitudes. *J. geophys. Res.* **85**, 6263–6268.
Turcotte, D. L. & Schubert, G., 1982. *Geodynamics*. Wiley, New York.
Turner, F. J., Griggs, D. T. & Heard, H. 1954. Experimental deformation of calcite crystals. *Bull. geol. Soc. Am.* **65**, 883–934.
Willis, B. 1894. Mechanics of Appalachian structure. *13th A. Rep. U.S. geol. Surv.*, 1891–92. 213–281.

APPENDIX 1: DESCRIPTION OF TEST RIG AND METHOD OF DATA ANALYSIS

The apparatus used in testing silicone putty is shown, schematically, in Fig. 14. The main element of the apparatus is an annular shear device made up of a load block, within which is drilled a vertical, cylindrical hole (diam. 25.4 mm), and a free cylindrical rod (diam. 15.9 mm) aligned along the hole axis. Material under test is packed tightly into the annular space between the block and rod. Shear of this material parallel to the axis of the annulus is produced by linear displacement of the rod driven by the combined weight of the rod, a known weight (varied from test to test), which is suspended below the shaft, and the core of a Linear Voltage Displacement Transducer, attached to the end of the load line. The outer coil housing of the LVDT and the outer block of the shear device are rigidly connected to a solid frame, and elastic distortion of the frame and elastic stretch within the load line are negligible. The output signal of the LVDT therefore provides a direct measure of the displacement of the rod relative to the block surrounding the test annulus. The LVDT is linear

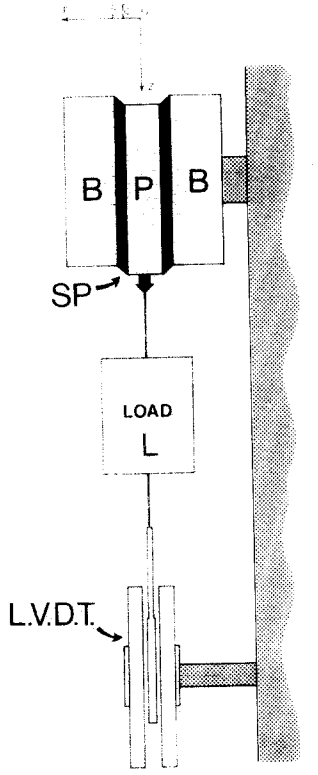

Fig. 14. Schematic cross-section of the annular shear rig employed to obtain rheologic data on silicone putty. B, block with vertical, cylindrical hole; R, cylindrical rod coaxial with hole in block B; SP, silicone putty packed into test anulus; L, load (variable from test to test). LVDT, linear voltage displacement transducer. Core of LVDT is attached to load line and moves downward with the rod R as the test proceeds. Stipple indicates rigid framework of apparatus. Coordinate axes (r, z) are referred to in text.

within ±0.01% over a displacement range of ±25 mm from the null position. Each test is initiated by manually releasing the load line, transferring load to the rod. The weight of the rod alone produces no detectable creep within the test material. Output from the LVDT is directed to a chart recorder to give a rod displacement/time creep curve at constant axial load.

In an analysis of the test data in terms of either elastic or creep properties, it is necessary to take into account the existence of a linear gradient in stress with radial distance within the test annulus. Strictly, account should also be taken of conditions at the free surfaces of the annulus but these will be ignored. Expressed in a radial coordinate frame (r, θ, z—Fig. 14), the radial gradient in shear stress σ_{rz} is given by

$$\sigma_{rz} = \frac{L}{2\pi l} \frac{1}{r} \tag{1}$$

where L = load, l = rod length (10 cm) and r = radial distance.

The shear strain e_{rz} (or strain rate $\dot{e}_{rz}$) at any point within the annulus cannot be measured directly. Deformation of the test material can only be monitored by a 'bulk' shear strain $\dot{e}_{rz}$ representing shear strain integrated across the full width of the annulus.

Now,

$$\dot{e}_{rz} = \frac{W}{(r_1 - r_0)} = \frac{1}{(r_1 - r_0)} \int_{r_0}^{r_1} \dot{e}_{rz}\, dr \tag{2a}$$

and

$$e_{rz} = \frac{W}{(r_1 - r_0)} = \frac{1}{(r_1 - r_0)} \int_{r_0}^{r_1} e_{rz}\, dr, \tag{2b}$$

where W is the relative displacement of points on the inner and outer surfaces of the annulus.

In equations (2a) and (2b), e_{rz}, $\dot{e}_{rz}$ represent total (or finite) strain; $\dot{e}_{rz}$, $\dot{e}_{rz}$ represent incremental strain rates.

The 'bulk' strain terms $\dot{e}_{rz}$ and $\dot{e}_{rz}$ can be obtained directly from creep curves representing shaft displacement as a function of time, under constant axial load. It is clear, however, that these data do not define conventional constant stress creep curves. It is necessary to treat the

data so as to obtain relationships between local strain, time and local stress at some radius, r. The procedure is relatively straightforward where the behaviour of interest involves a linear relationship between stress and recoverable strain (Linear Elastic) or between stress and strain rate during creep (Newtonian Viscous). The following relationships can be derived from these cases.

Linear Elastic:

$$e_{rz} = \frac{1}{G}\sigma_{rz}, \text{ where } G = \text{ridigity modulus.}$$

At $r = r_a = \dfrac{r_1 + r_0}{2}$,

$$e_{rz} = C\hat{e}_{rz}. \tag{3a}$$

Linear Newtonian Viscous:

$$\dot{e}_{rz} = \frac{1}{\mu}\sigma_{rz},$$

where μ = shear viscosity modulus.

At $r = r_a = \dfrac{r_1 + r_0}{2}$,

$$\dot{e}_{rz} = C\dot{\hat{e}}_{rz}. \tag{3b}$$

In both (3a) and (3b),

$$C = \frac{(r_1 - r_0)}{r_a} \ln \frac{r_1}{r_0}.$$

A third case of interest, which is also amenable to analysis, is that of a material which shows power-law creep behaviour, i.e. strain rate, measured at a reference level of total strain beyond the elastic limit, is proportional to stress raised to some power n.

Power Law Creep:

$$\dot{e}_{12} = A\sigma^n,$$

where A is constant for constant experimental conditions (temperature, strain, material structure, etc.).

At $r = r_a = \dfrac{r_1 + r_2}{2}$,

$$\dot{e}_{rz} = K\dot{\hat{e}}_{rz}, \tag{3c}$$

where

$$K = (n - 1)\frac{(r_1 - r_0)}{r_a}\left[\frac{r_0}{(r_a^{n-1} - r_0^{n-1})}\right].$$

It can be seen that, in each case, local strain parameters (e.g. at the mid-point of the annulus) can be derived from measurable 'bulk' strain parameters and the known radii r_0 and r_1. It should also be noted that materials showing a linear or power-law dependence of a given local strain parameter ($e_{rz}, \dot{e}_{rz}$) on stress will show the same type of functional relationship between equivalent bulk strain parameters ($\hat{e}_{rz}, \dot{\hat{e}}_{rz}$) and stress.

Linear Elastic:

$$\hat{e}_{rz} = \frac{1}{\hat{G}}\sigma_{rz}$$

at $r = r_a$, where

$$\hat{G} = G\frac{(r_1 - r_0)}{r_a \ln\left(\dfrac{r_1}{r_0}\right)}. \tag{4a}$$

Linear Newtonian Viscous:

$$\dot{\hat{e}}_{rz} = \frac{1}{\hat{\mu}}\sigma_{rz}$$

at $r = r_a$ where

$$\hat{\mu} = \mu\frac{(r_1 - r_0)}{r_a \ln\left(\dfrac{r_1}{r_0}\right)}. \tag{4b}$$

Power Law Creep:

$$\dot{\hat{e}}_{rz} = \hat{A}\sigma_{rz}^n$$

where

$$\hat{A} = A\frac{r_a^n}{(r_1 - r_0)}(n - 1)\left[\frac{(r_1^{n-1} - r_0^{n-1})}{(r_1 r_0)^{n-1}}\right]. \tag{4c}$$

As a first step in analysing data, therefore, a test for linearity or power-law dependence in a particular rheological relationship can be made by plotting bulk strain or strain rate against stress at any point within the annulus.

APPENDIX 2: RHEOLOGIC PROPERTIES OF SILICONE PUTTY AND PLASTICINE

Test results for silicone putty SP4

Elastic properties. Rod displacement/time creep curves do not show a well defined 'instantaneous' elastic response on the initial application of load. This is illustrated in Fig. 9 taken from a test in which the silicone putty in the annulus was cyclically loaded and unloaded to study the strain relaxation characteristics of the silicone putty (see caption for details). The material does, however, sustain a significant amount of primary creep which is recovered on unloading.

Given the difficulty in measuring an 'instantaneous' elastic response, it is not possible to derive a true elastic rigidity modulus from the test data. We can, however, analyse the relationship between total recoverable elastic strain $\hat{e}_{rz}$ and stress and in Fig. 10 we show this relationship graphically (using stress σ_{rz} at $r = (r_0 + r_1)/2$ as the reference stress level). The data yield reasonable agreement to a linear relationship. This being the case, equation (3a) can be used to compute 'true' local elastic strain e_{rz} ($r = (r_0 + r_1)/2$). However, the resulting shift that should be applied to the best fit line to the 'bulk' strain data on the basis of this assumption is insignificant (the shifted line would fall within the scatter of data points on Fig. 10). A rigidity modulus relating total recoverable strain to stress computed from the slope of line on Fig. 10 has the value 10 kPa.

Creep properties. As a first step in studying the dependence of rate of deformation, during creep, on applied stress, the rod displacement creep curves were analysed to define 'bulk' strain rate $\dot{\hat{e}}_{rz}$ at a 'bulk' shear strain of 0.2 (corresponding to a rod displacement of 0.95 mm, given that the annulus is 4.75 mm wide). Taking σ_{rz} at the mid-point of the annulus as the reference shear stress, 'bulk' shear strain-shear stress data have been graphed using logarithmic axes. The results are shown in Fig. 11 for data obtained for three temperature ranges (T = 18 ± 1°C; T = 22 ± 1°C and T = 26 ± 1°C). Inspection of data points measured from the 18°C tests clearly shows that the constitutive relationship between 'bulk' strain rate and stress is neither linear nor power-law when considered over the full range of strain rate accessed in the tests. It proved impossible to obtain any sensible flow law which could adequately fit the relationship between bulk strain rate and shear stress represented by the data. This problem generated a related problem in determining the 'shift' necessary to convert the 'bulk' strain rate used in constructing Fig. 11 into true local strain rate at the center of the annulus. It is necessary to determine such a flow law in order to enable the calculation of the data point shift.

We note, at this point, that in using the annular test rig, it was initially anticipated that silicone putty would obey a constitutive relationship with a linear or approximately linear dependence of strain rate on stress. This result was obtained by workers in the centrifuge laboratory at Uppsala, Sweden and was reported by Ramberg (1967) who defined the silicone putties they used as Newtonian viscous. We also note that, in the absence of any empirically defined flow relationship, it would be possible to apply a precise shift to bulk strain data, to yield local strain rate parameters, if the apparatus had been designed so as to allow variation in annular width from test to test. It can be shown that

$$\dot{e}_{rz}\ (\text{at } r = r_1) = (r_1 - r_0)\frac{\partial \dot{\hat{e}}_{rz}}{\partial r} - \frac{1}{2}\dot{\hat{e}}_{rz}. \tag{5}$$

Equation (5) has the following significance. Given a series of tests with r_0 fixed, load L fixed and r_1 as the test variable, then it would be possible to define the gradient $\partial\dot{\hat{e}}_{rz}/\partial r$, and a corresponding 'bulk' strain rate $\dot{\hat{e}}_{rz}$, for a particular value of r_1. Equation (5) could then be used to define local strain rate, $\dot{e}_{rz}$, under the given load conditions, at this value of radius (r_1). As has been indicated, an equivalent procedure cannot be carried out when load is the test variable.

Given this problem, the method we have used to convert from 'bulk' to 'local' strain rate involves (i) defining best-fit curves to the data points (heavy lines in Fig. 11). The form of these curves was constrained in part by evidence, discussed later, for a finite yield strength and for an interpreted approach to linearity in stress–strain rate dependence at strain rates in excess of 10^{-1} s^{-1}. (ii) The slope of the resulting curve was measured at a series of points and used to define a parameter $n = \mathrm{d}(\log \dot{e}_{rz})/\mathrm{d}(\log \sigma_{rz})$. (iii) The value of n at each point on the curve was then introduced into equation (3c) to compute the local magnitude of the 'shift' required to convert from 'bulk' to 'local' strain rate. The results of this adjustment procedure are shown by the fine curves in Fig. 11. The effects of the curve shifts can be seen to be relatively insignificant. We have not been able to prove the validity of this procedure algebraically. It can be strictly justified only where there is a power law dependence of strain rate on stress over a finite range of strain rate.

Given the uncertainty in fitting curves to the data point spread, we would suggest that the shifted curves give a reasonable indication of the flow behaviour of the material. It is unlikely that adjustments significantly in excess of those shown would be required for any rational type of flow law. The data are certainly adequate to allow a reasonable interpretation of the validity of the material as an analogue for the deformation behaviour of incompetent strata (e.g. shales) within natural sedimentary sequences.

In Fig. 11 the 18°C test results are extrapolated to strain rates below 10^{-4} s^{-1} and in excess of 10^{-1} s^{-1}. Tests carried out in the shear rig yield data over a range in strain rate from 10^{-4} s^{-1} to 10^{-1} s^{-1}. The results show a progressive increase in non-linearity with decrease in strain rate. This tendency is confirmed by the fact that material within the test annulus shows no detectable rate of creep ($\dot{e}_{rz} < 10^{-7}$ s^{-1}) under load from the rig rod alone (σ_{rz}, at $r = (r_1 + r_0)/2$, $= 3 \times 10^2$ Pa). In terms of measurable strain rates, SP4 therefore exhibits a finite yield strength corresponding to 3×10^2 Pa maximum shear stress.

The extrapolation to linear behaviour at relatively high strain rates is based on evidence which involves a consideration of the flow characteristics of Plasticine, the competent component of the model multilayers.

Properties of Plasticine

Data on the flow properties of three grades of Harbutt Plasticine have been reported by McClay (1976). These tests were carried out in a pure shear deformation rig, described by Cobbold (1975), and involved testing at constant strain rate for strain rates ranging from 10^{-6} to 10^{-3} s^{-1}. McClay measured flow stress at 10% shortening and plotted stress as a function of strain rate for tests carried out on various grades of Plasticine, at two temperatures (25°C, 45°C). The grade relevant to this discussion is Harbutt's Standard White Plasticine, which is the material closest to the Harbutt Gold Medal brand in our work. Data shown by McClay (1976, fig. 2), for this grade at 25°C, have been converted to shear stress and shear strain rate and plotted in Fig. 12 (curve labelled P). McClay found that the flow behaviour of this Plasticine grade can be adequately defined by a power law dependence of strain rate on stress with a stress exponent within the range $n \approx 6$–9. This figure also incorporates the adjusted data for silicone putty SP4 defined in Fig. 11.

We have indicated above that the success of the construction technique we use in producing silicone putty–Plasticine multilayers is due to the low contrast in flow strength between the two materials at strain rates induced by rolling. Deformation rates under rolling conditions are difficult to estimate but are unlikely to exceed 10^1 s^{-1}.

Given these observations, extrapolation of the curves shown in Fig. 12 must produce strength convergence at shear strain rates of the order 10^1 s^{-1}, if the roll rate estimate is correct. The most reasonable interpretation is to assume an approach to Newtonian behaviour for the putty at strain rates in excess of 10^{-1} s^{-1}. It should be noted that this interpretation might also explain the discrepancy between our results and the Newtonian behaviour reported by Ramberg (1967), if Ramberg's tests were carried out at relatively fast strain rates. Ramberg does not indicate the range of strain rate over which the tests were conducted. As mentioned in the text, the discrepancy could also be related to differences in the type of putty used.

If the validity of the extrapolation to high strain rate shown in Fig. 12 is accepted, there is still a problem related to the zone at which convergence occurs. A simple extrapolation of McClay's data to high strain rate would indicate convergence at a shear strain rate of 10^2 s^{-1}, a rate we believe is in excess of deformation rates induced during multilayer rolling. This observation would imply that either (i) stress levels documented by McClay are too high (possibly by as much as an order of magnitude), perhaps due to machine friction, or (ii) a simple linear extrapolation of McClay's data to strain rates in excess of 10^{-1} s^{-1} is unjustified.

Two additional observations would support the suggestion that a simple extrapolation of the linear fit defined by McClay to high strain rates is not valid. (a) Such an extrapolation would yield a uniaxial compressive stress of 1 MPa at a shortening rate of 10^{-2} s^{-1}. This level of stress seems to exceed the strength experienced in handling, rolling and moulding this material. (b) Stevens (1983) carried out a centrifuge model study, using Gold Medal plasticine to simulate and analyse failure of embankment slopes. Failure occurred on rotational shear surfaces of the type discussed in standard works on slope failure in soils (e.g. Terzaghi & Peck 1967). He used conventional methods of analysis of this type of failure phenomenon to define a yield strength for plasticine under centrifuge conditions. Results, based on six experiments, gave a yield strength in the range 6.6×10^4–9.5×10^4 Pa. Rates of deformation involved in the generation of shear failure in these experiments are difficult to estimate. However, measurements on the dimensions of and strain within failure zones and observations on rates of slope failure would suggest shear strain rates of the order 10^{-2}–10^0 s^{-1} as a reasonable estimate. The stippled region in Fig. 12 defines the estimated range of conditions indicated by Stevens' observations. On the basis of these observations we have constructed line P′ on Fig. 12 as representing our preferred estimate of the stress–strain rate relationship for the Plasticine we have used.